Journal of Alloys and Compounds 509 (2011) 9659–9662

Contents lists available at ScienceDirect

Journal of Alloys and Compounds

journal homepage: www.elsevier.com/locate/jallcom

Transport mechanism in a ceramic system: $LiCo_{3/5}Fe_{1/5}Cu_{1/5}VO_4$

Moti Ram*

Department of Physics and Meteorology, Indian Institute of Technology, Kharagpur, West Bengal, 721302, India

ARTICLE INFO

Article history:
Received 28 April 2011
Received in revised form 20 July 2011
Accepted 21 July 2011
Available online 28 July 2011

Keywords:
Ceramics
Chemical method
X-ray diffraction
Impedance spectroscopy
Transport phenomena

ABSTRACT

The electrical impedance and modulus properties of a $LiCo_{3/5}Fe_{1/5}Cu_{1/5}VO_4$ ceramic system were measured by impedance spectroscopy method in the frequency range 10^2–10^6 Hz and temperature range 22–250 °C. X-ray diffraction study reveals formation of the compound in a cubic crystal system with lattice parameters $a = 8.2756\ (3)$ Å. Field emission scanning electron microscopy is used to investigate the grain morphology of the material. Nyquist plots confirm the existence of bulk and grain boundary effects at 22 °C ≤ T ≤ 200 °C, and bulk, grain boundary and polarization effects at T ≥ 225 °C. Electrical modulus study indicates a non-Debye behavior of the material. A detailed study of bulk conductivity shows electric conduction in the material as a thermally activated process.

1. Introduction

Recently, lithiated transition metal oxides are of considerable interest for their potential technological applications such as cathode materials in lithium ion batteries [1–6], supercapacitors [7,8], microwave frequency applications [9], etc. Electrical conductivity measurements have been considered as an important tool for studying the ionic transport properties of these materials. Several processes like ion movement through the bulk of the electrolyte, charge transfer across the electrode–electrolyte interface, etc. take place when electrical current passes through such materials [10–12]. These processes respond to the applied electric field in the different frequency ranges because of different relaxation times for each process. Electrode polarizations become significant at very low frequencies while ionic migration losses take place at high frequencies. Complex impedance (Z^*) analysis have been widely used to identify these individual processes, and the data have been analyzed using the formalism ($M^* = 1/\varepsilon^* = M' + jM'' = j\omega C_o Z^*$), where $Z^* = Z' - jZ''$, C_o (vacuum capacitance of the cell without sample) $= \varepsilon_o A/t$, M^* = complex modulus, ε^* = complex permittivity, M' = real part of M^*, M'' = imaginary part of M^*, Z' = real part of Z^*, Z'' = imaginary part of Z^*, $j = (-1)^{1/2}$, ω = angular frequency, ε_o = permittivity of free space, A = effective area of the electrode and t = thickness of the sample [13]. This formalism has shown electrical relaxations in the materials with distribution of relaxation times. Several such types of studies have been reported for lithiated transition metal oxides [14–23]. This was motivated to prepare a $LiCo_{3/5}Fe_{1/5}Cu_{1/5}VO_4$ compound and characterize its electrical impedance and modulus properties. In the present investigation, a systematic study on structural, electrical impedance and modulus properties of the compound ($LiCo_{3/5}Fe_{1/5}Cu_{1/5}VO_4$) has been undertaken. Electrical impedance and modulus properties of this compound have been studied using complex impedance spectroscopy technique.

2. Experimental procedures

2.1. Material preparation

Solution-based chemical route was used to prepare $LiCo_{3/5}Fe_{1/5}Cu_{1/5}VO_4$ fine powder. The required chemicals were $LiNO_3$, $Co(NO_3)_2{\cdot}6H_2O$, $Cu(NO_3)_2{\cdot}3H_2O$, $FeCO_3$, NH_4VO_3, triethanolamine (TEA), HNO_3 and oxalic acid. The stoichiometric amounts of highly pure $LiNO_3$, $Co(NO_3)_2{\cdot}6H_2O$, $Cu(NO_3)_2{\cdot}3H_2O$, $FeCO_3$ and NH_4VO_3 were dissolved in distilled water and mixed together. $FeCO_3$ was dissolved in warm distilled water in the presence of oxalic acid. Thereafter TEA was added maintaining a ratio of 3:1 with metal ions. HNO_3 and oxalic acid were added to dissolve the precipitate and then the clear solution was evaporated at ~200 °C temperature with continuous stirring. A fluffy, mesoporous and carbon-rich precursor mass was formed by complete evaporation of the solution. After grinding, the voluminous, fluffy and black carbonaceous mass was calcined at 550 °C for 3 h to produce the desired phase, which is confirmed by X-ray diffraction analysis. The calcined powder was cold pressed into circular disc shaped pellets of diameter 12–13 mm and various thicknesses with polyvinyl alcohol as the binder using hydraulic press at a pressure ~7.85–9.81 MPa. These pellets were then sintered at 575 °C for 2 h followed by slow cooling process. Subsequently, the pellets were polished by fine emery paper to make their faces smooth and parallel. The pellets were finally coated with conductive silver paint and dried at 150 °C for 3 h before carrying out electrical measurements.

* Tel.: +91 3222 281902.
E-mail address: motiram05@yahoo.co.in

0925-8388/$ – see front matter © 2011 Elsevier B.V. All rights reserved.
doi:10.1016/j.jallcom.2011.07.072

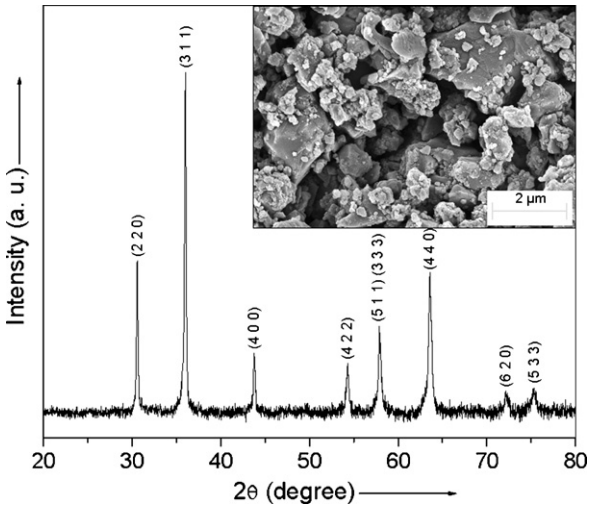

Fig. 1. X-ray diffraction pattern and field emission scanning electron micrograph (inset) of $LiCo_{3/5}Fe_{1/5}Cu_{1/5}VO_4$ at room temperature.

2.2. Material characterization

X-ray diffraction of the calcined powder was studied at room temperature using a diffractometer (PANalytical PW 3040/60 X'Pert PRO) in the angle range $20^\circ \leq 2\theta \leq 80^\circ$ on being irradiated by Cu K_α radiation of wavelength equal to 1.5419 Å. The surface morphology of the gold-sputtered sample was recorded with different magnifications at room temperature using a ZEISS (Model: SUPRA™ 40) field emission scanning electron microscope. Electrical impedance, phase angle, tangent loss and capacitance were measured by applying a voltage ~0.701 V using a computer-controlled frequency response analyzer (HIOKI LCR Hi TESTER, Model: 3532-50) with varying temperature over the frequency range 10^2–10^6 Hz.

3. Results and discussion

Fig. 1 shows the X-ray diffraction spectrum of $LiCo_{3/5}Fe_{1/5}Cu_{1/5}VO_4$ at room temperature. The diffractogram reveals the formation of a highly crystalline phase of the product. Standard computer software (POWD MULT) [24] is used to analyze the X-ray diffraction data. X-ray diffraction study exhibits a cubic unit cell structure of the compound with lattice parameters $a = 8.2756\ (3)$ Å, which are refined by a least squares refinement method. The values of the indexed peaks are given in Table 1. Furthermore, measured density of the compound is worked out to be 95.86% of theoretical density.

Field emission scanning electron micrograph at room temperature of the surface of gold-sputtered sintered pellet sample is shown in Fig. 1(inset). It is seen from the micrograph that grains present an average grain size with polydisperse distribution on the surface of sample. The grain size of the compound is ~0.2–3.0 μm.

Table 1
X-ray diffraction data of $LiCo_{3/5}Fe_{1/5}Cu_{1/5}VO_4$.

Diffraction angle 2θ (°)	d-spacing (in Å)		Miller indices			Rel. intensity (I/I_o) [%]
	d_{obs}	d_{cal}	h	k	l	
30.58	2.9231	2.9259	2	2	0	45.42
36.01	2.4937	2.4952	3	1	1	100.00
43.75	2.0690	2.0689	4	0	0	18.55
54.30	1.6895	1.6892	4	2	2	15.52
57.89	1.5929	1.5926	5	1	1	26.37
			3	3	3	
63.57	1.4635	1.4629	4	4	0	42.03
72.14	1.3093	1.3085	6	2	0	7.58
75.37	1.2611	1.2620	5	3	3	8.43

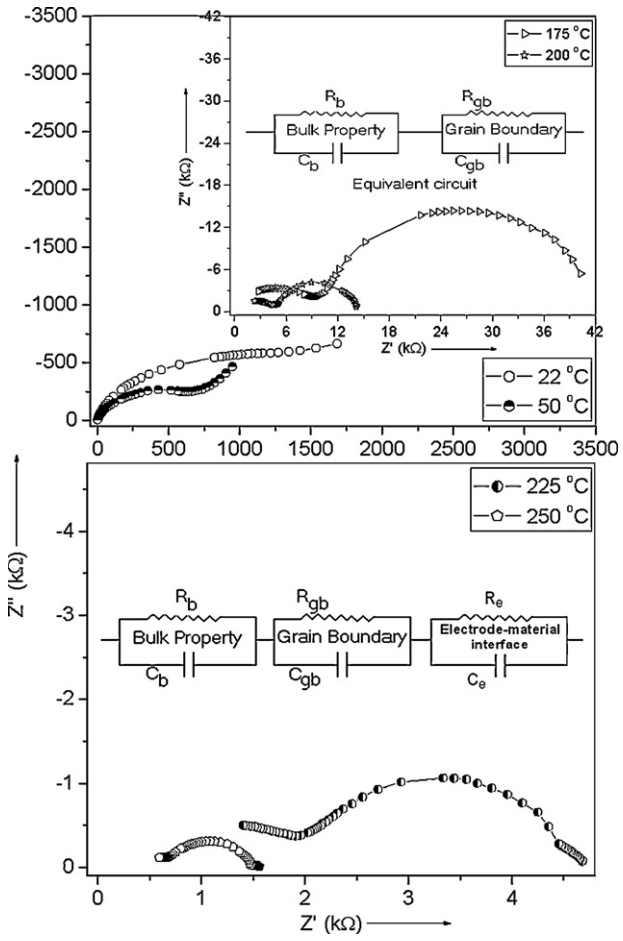

Fig. 2. Nyquist plots at different temperatures with electrical equivalent circuit (inset).

Furthermore, micrograph indicates a polycrystalline texture of the compound.

Fig. 2 shows the Nyquist plots (i.e., Z′ verses Z″ graphs) at different temperatures. These are characterized by depressed semicircles, whose centers are below the real axis. This decentralization follows Cole–Cole's formalism: $Z^*(\omega) = R/1 + (j\omega/\omega_o)^{1-n}$, where the depressed semicircle represents typically a phenomenon with a distribution of relaxation times (i.e., non-Debye type relaxation phenomenon), and n lies between 0 and 1 and represents the magnitude of the departure of electrical response from an ideal condition having a single relaxation time, or represents the distribution of relaxation times [20,25,26]. This relation gives the classical Debye formalism for $n = 0$. Such type of non-ideal behavior is correlated to several factors as the grain size distribution, grain orientation, grain boundaries, etc. The existence of the distribution of relaxation times is correlated to some depression degree (β), which is related to n by an equation ($n = 2\beta/\pi$) [20,25,26]. The depressed semicircles at high, middle and low frequency regions arise due to the bulk, grain boundary and polarization (polarization at the electrode–material interface) effects, respectively [13]. It is seen from Fig. 2 that, double and triple depressed semicircles are observed at $22\,^\circ\text{C} \leq T \leq 200\,^\circ\text{C}$ and $T \geq 225\,^\circ\text{C}$, respectively. The presence of double depressed semicircles in the pattern indicates that electrical conduction in the material takes place due to bulk and grain boundary effects, and modeled by an equivalent circuit (series combination of two parallel R–C circuits) [13,20,26–28]. The occurrence of triple depressed semicircles in the pattern shows that electrical conduction in the material is taking place due to

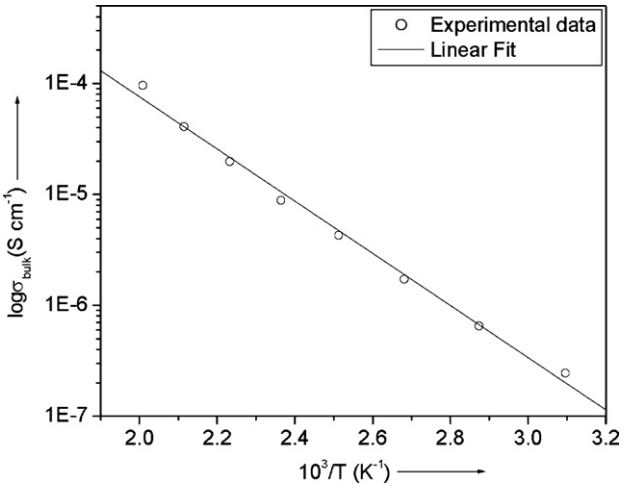

Fig. 3. Variation of σ_{bulk} as a function of temperature.

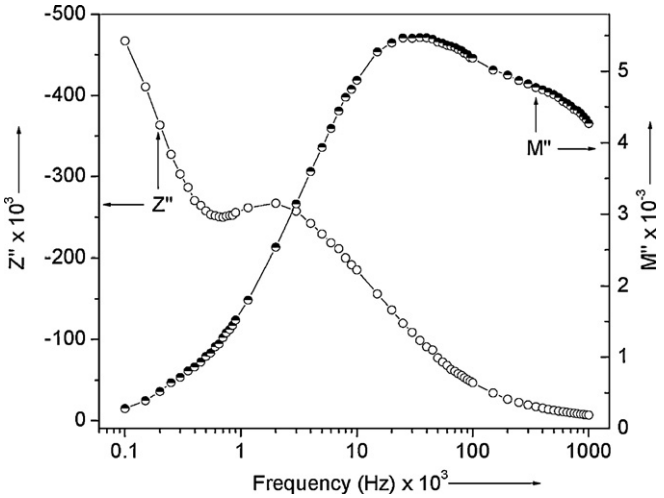

Fig. 4. Frequency dependence of Z'' and M'' at 50 °C of the system.

bulk, grain boundary and polarization effects, and modeled by an equivalent circuit (series combination of three parallel *R–C* circuits) [13,26–28]. The corresponding electrical equivalent circuits are presented in Fig. 2(inset). Furthermore, the intercept of semicircular arc on the real axis shifts toward the origin with rise in temperature, which indicates a reduction in resistive behavior of the material. Thus, bulk conductivity (σ_{bulk}) of the material increases with rise in temperature. The σ_{bulk} has been estimated from the bulk resistance (R_b) obtained from Nyquist plots using the relation ($\sigma_{bulk} = t/A\,R_{b)}$, where t = thickness of the sample and A = effective area of the electrode. It is also seen from Fig. 2 that semicircular arcs deviate from their perfect semicircular arcs, which indicates the presence of mixed conduction (i.e., ionic and electronic conduction) in the material [29,30]. In such a case, σ_{bulk} is a combined effect arising out of both electrons (and or holes) and ions. Therefore $\sigma_{bulk} = \sigma_{ion} + \sigma_{dc} = \sigma_{ion} + \sigma_{elec,}$ where σ_{dc} = d.c. conductivity, σ_{ion} = ionic conductivity and σ_{elec} = electronic conductivity [29,31]. The increasing nature of σ_{bulk} with temperature is shown in Fig. 3. This plot (Fig. 3) follows an Arrhenius relation [$\sigma_{bulk} = \sigma_o \exp(-E_a/kT)$], where σ_o = pre-exponential factor corresponding to $1/T = 0$, E_a = activation energy for charge transfer, k = Boltzmann constant and T = absolute temperature [29,31]. This type of feature suggests that electric conduction in the material is a thermally activated process. The value of E_a with the help of Arrhenius relation and slope of Fig. 3 is estimated as ~(0.467 ± 0.015 eV at 50–225 °C).

The variation of Z'' and M'' with frequency at 50 °C is shown in Fig. 4. It is seen from figure that $Z''_{max.}$ and $M''_{max.}$ are not occurring at same frequency, and a broad modulus spectra is obtained, which is an indication of wide distribution of relaxation times. Furthermore, Z'' and M'' spectra are broadened on low and high frequency side of the peak maximum, respectively. These features suggest about non-Debye behavior of the material [32].

Fig. 5 shows the frequency dependence of M' at different temperatures. It is observed that M' reaches a maximum constant value $M_\infty = 1/\varepsilon_\infty$ at high frequencies, and approaches to zero at low frequencies that confirm the presence of an appreciable ionic polarization at studied temperatures [33]. Also, M' levels off at high frequencies and temperatures due to the relaxation processes, which spread over a range of frequency.

Frequency dependence of M'' at different temperatures is presented in Fig. 6. The value of M'' increases with rise in frequency and reaches to peak value at a particular frequency. This frequency is known as relaxation frequency ($f_{max.}$), which corresponds to $M''_{max.}$. The position of the peak shifts toward the high frequency

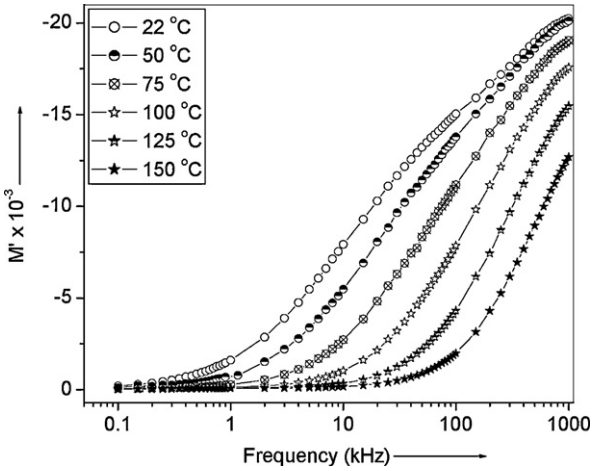

Fig. 5. Frequency dependence of M' at different temperatures.

side on increasing temperature. This behavior suggests about the presence of electrical relaxation process in the material with temperature dependence of relaxation time. The frequency region below $f_{max.}$ determines the range in which charge carriers move to long distances. At frequencies above $f_{max.}$, the charge carriers

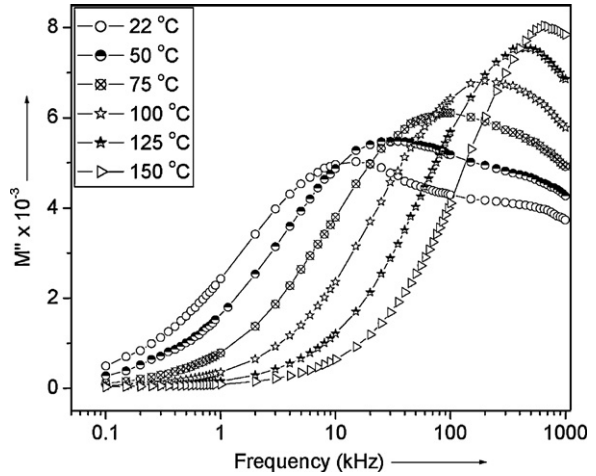

Fig. 6. Frequency dependence of M'' at different temperatures.

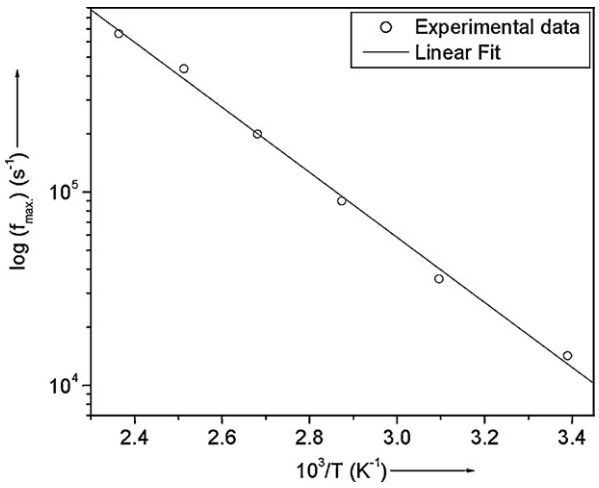

Fig. 7. Variation of relaxation frequency ($f_{max.}$) as a function of temperature.

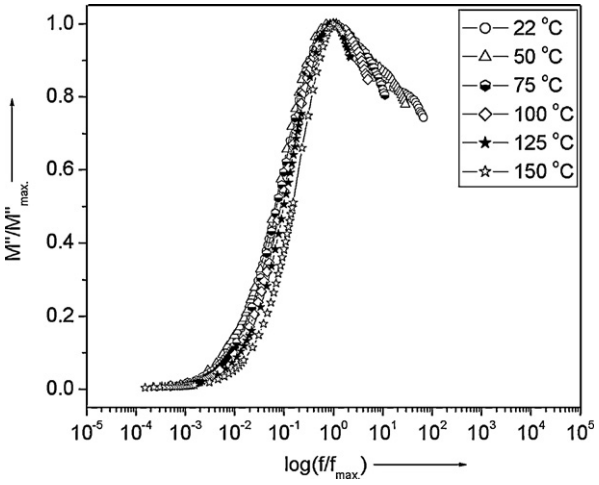

Fig. 8. The variation of $M''/M''_{max.}$ with $\log(f/f_{max.})$ at different temperatures.

move to short distances and confine to potential wells [20]. Furthermore, asymmetric broadening of the peak with temperature-rise indicates non-unique (i.e., multiple) relaxation-timescale (i.e., non-Debye type relaxation) [20]. The $f_{max.}$ relates with relaxation time (τ_σ) as $\tau_\sigma 2\pi f_{max.} = 1$. The variation of $\log(f_{max.})$ with $10^3/T$ is shown in Fig. 7. The increasing nature of $f_{max.}$ with temperature indicates that relaxation mechanism is a thermally activated process. It obeys the Arrhenius relation [$f_{max.} = f_o \exp(-E_a/kT)$], where f_o = pre-exponential factor, E_a = activation energy, k = Boltzmann constant and T = absolute temperature [33]. The value of E_a for this relaxation process is calculated as ~(0.334 ± 0.011 eV at 22–150 °C).

The scaling behavior of the material has been explained by $M''/M''_{max.}$ verses $\log(f/f_{max.})$ plots at different temperatures (Fig. 8). Here, each M'' and frequency for different temperatures have been scaled by $M''_{max.}$ and f_{max}, respectively. This broad asymmetric pattern indicates about non-Debye type relaxation phenomena in the material. The nearly perfect overlap of the modulus curves with coincidence of peaks for all temperatures indicates that dynamical processes occurring at different frequencies are independent of temperature with non-Debye type (polydispersive) of conductivity relaxation [20,34]. This is an indication of a distribution of relaxation times in the conduction process [35], and the movement of ions via hopping mechanism [20,36].

4. Conclusions

The prepared compound [$LiCo_{3/5}Fe_{1/5}Cu_{1/5}VO_4$] is a new ceramic system, which has been synthesized by solution-based chemical method. X-ray diffraction results reveal a cubic crystal system with lattice parameters $a = 8.2756\,(3)$ Å. Microstructure study indicates a polycrystalline texture of the compound with grains of unequal sizes ~0.2–3.0 μm. Impedance plots show electrical conduction in the material due to the bulk, grain boundary and polarization effects. The modulus plots show a non-Debye type behavior of the material. The distribution of relaxation times in the conduction process is indicated by broad modulus spectrum. Bulk conductivity study shows about the electric conduction in the material as a thermally activated process.

Acknowledgements

The author is grateful to the Nanomaterials Laboratory of the Department of Chemistry and Central Research Facility, Indian Institute of Technology, Kharagpur-721302 (W.B.), India, for providing facilities to conduct experiments.

References

[1] M.N. Obrovac, O. Mao, J.R. Dahn, Solid State Ionics 112 (1998) 9.
[2] Y. Sakurai, H. Arai, J. Yamaki, Solid State Ionics 113–115 (1998) 29.
[3] L.H. Chi, N.N. Dinh, S. Brutti, B. Scrosati, Electrochim. Acta 55 (2010) 5110.
[4] M.V. Reddy, A. Levasseur, J. Electroanal. Chem. 639 (2010) 27.
[5] G.M.K. Jr., I. Belharouak, H.M. Wu, K. Amine, Electrochim. Acta 56 (2011) 1426.
[6] N. Dupre, J.F. Martin, J. Oliveri, P. Soudan, A. Yamada, R. Kanno, D. Guyomard, J. Power Sources 196 (2011) 4791.
[7] J.S. Pena, O. Crosnier, T. Brousse, Electrochim. Acta 55 (2010) 7511.
[8] C.V. Rao, B. Rambabu, Solid State Ionics 181 (2010) 839.
[9] J.R. Dahn, U.V. Sacken, C.A. Michal, Solid State Ionics 44 (1990) 87.
[10] M. Ram, Phys. B 405 (2010) 602.
[11] P.P. Hankare, R.P. Patil, U.B. Sankpal, K.M. Garadkar, R. Sasikala, A.K. Tripathi, I.S. Mulla, J. Magn. Magn. Mater. 322 (2010) 2629.
[12] M. Ram, J. Alloys Compd. 509 (2011) 5688.
[13] E. Barsoukov, J.R. Macdonald, Impedance Spectroscopy—Theory, Experiment, and Applications, John Wiley & Sons, New Jersey, 2005.
[14] P.V. Reddy, T.S. Rao, J. Less Common Met. 79 (1981) 191.
[15] S.A. Mazen, Phys. Status Solidi (a) 154 (1996) 681.
[16] A. Ahmed, J. Mater. Sci. 27 (1992) 4120.
[17] S.A. Mazen, F. Metawe, S.F. Mansour, J. Phys. D: Appl. Phys. 30 (1997) 1799.
[18] M. Ram, S. Chakrabarti, J. Phys. Chem. Solids 69 (2008) 905.
[19] M. Ram, Mater. Chem. Phys. 109 (2008) 465.
[20] M. Ram, Solid State Ionics 178 (2008) 1922.
[21] M. Ram, Curr. Appl. Phys. 10 (2010) 1013.
[22] M. Ram, Phys. B 405 (2010) 2205.
[23] M. Ram, J. Alloys Compd. 509 (2011) 1744.
[24] E. Wu, POWD MULT: An Interactive Powder Diffraction Data Interpretation and Indexing Program, Version 2. 1, School of Physical Sciences, Flinder University of South Australia, Bardford Park, SA, Australia, 1989.
[25] M.A.L. Nobre, S. Lanfredi, J. Phys. Chem. Solids 64 (2003) 2457.
[26] M. Ram, J. Alloys Compd. 488 (2010) 306.
[27] A.P. Barranco, F.C. Pinar, O.P. Martinez, J.D.L.S. Guerra, I.G. Carmenate, J. Eur. Ceram. Soc. 19 (1999) 2677.
[28] S. Brahma, R.N.P. Choudhary, A.K. Thakur, Phys. B 355 (2005) 188.
[29] T. Matsuo, T. Yagami, T. Katsumata, J. Appl. Phys. 74 (1993) 7264.
[30] K. Singh, Solid State Ionics 93 (1997) 147.
[31] G.S. Murugan, K.B.R. Varma, Solid State Ionics 139 (2001) 105.
[32] K. Prabakar, S.P.M. Rao, J. Alloys Compd. 437 (2007) 302.
[33] K.S. Rao, D.M. Prasad, P.M. Krishna, B. Tilak, K.C. Varadarajulu, Mater. Sci. Eng. B 133 (2006) 141.
[34] P. Ganguly, A.K. Jha, K.L. Deori, Solid State Commun. 146 (2008) 472.
[35] M. Sural, A. Gosh, Solid State Ionics 130 (2000) 259.
[36] A. Kumar, B.P. Singh, R.N.P. Choudhary, A.K. Thakur, J. Alloys Compd. 394 (2005) 292.